Effect of NaClO disinfection/cleaning on passive films on AISI 316L

G. Tranchida[a], F. Di Franco[a*], S. Virtanen[b], M. Santamaria[a]

[a] Università degli Studi Palermo, Dipartimento di Ingegneria, Viale delle Scienze, Ed. 6, 90128, Palermo, Italy.
[b] Institute for Surface Science and Corrosion, Department of Material Science, Friederich Alexander Universtat Erlangen-Nuremberg

* Corresponding author
francesco.difranco@unipa.it

Abstract

316L stainless steel samples were passivated in NaClO containing solutions in order to simulate disinfection processes. Passive films were grown at the open circuit potential by immersion in NaClO aqueous solutions at different concentrations and temperature in order to understand, how exposure to aggressive environments could affect subsequent corrosion resistance of SSs. In the attempt to study the passive film growth mechanism, *in-situ* Open Circuit Potential measurements were performed in the same growth solutions. Photoelectrochemical and impedance investigation of passive films was carried out in order to link their solid state properties with their corrosion behaviour.

Keywords: stainless steel, EIS, polarization, XPS, passivity, transpassivity

1 - Introduction

Due to their mechanical properties and corrosion resistance, stainless steels are the most employed materials in food and pharmaceutical industries, where severe regulations relating to contamination of processed fluids and a highly awareness regarding health and safety of consumers are required. In order to avoid contaminations due to the occurrence of corrosion phenomena and to eliminate bacteria, viruses and spoilage microorganisms from surfaces and equipment, *Cleaning*, *Disinfection* and *Sanitization* operations are usually employed thanks to the physical action of high velocity flow jet spray, agitation and chemical action of cleaning agents enhanced by high temperature [1]. Storage vessels and distribution systems for purified water and clean steam in pharmaceutical industry can show red brown to dark violet deposits called rouge due to their visual appearance. Rouging can occur to different degree and according to different mechanisms [2-3]. Class I rouging occurs when rouge is a deposited corrosion product mainly constituted by iron oxi-hydroxides.

Class II rouge occurs when an adherent corrosion product originates *in-situ* on un-passivated or improperly passivated stainless steel surfaces, and it is promoted by Cr dissolution. Finally, Class III rouge is the result of an iron oxide corrosion product called magnetite (blue or black), usually formed on SS surfaces in high-temperature steam systems.

Sodium hypochlorite is the most widely used chemical in the food industry for the removal of organic soils (cleaning) and control of microbes (disinfection) in a single process. According to the literature [4-8], the disinfection is due to the penetration of HClO into microbial cell across their wall and membrane inhibiting the enzyme activity essential to the growth and damaging the membrane and DNA. The cleaning action of sodium hypochlorite is based on the synergism of the oxidizing power of ClO^- and the ability of OH^- to dissolve organic soils. A role is also played by the temperature [9-11].

The concentration of un-dissociated HClO and ClO^- are pH dependent according to the following relationships:

$HClO = ClO^- + H^+$

$\log [ClO^-]/[HClO] = - 7.49 + pH$

Thus, $[HClO] << [ClO^-]$ in alkaline solution. The concentration of NaClO has a direct impact on the pH of the solution but also on the possible disinfection activity. This explains why there are several works investigating the effect of NaClO solution with different concentration on their cleaning and disinfection activity. In spite the large interest of these aspects, there are just a few works focusing on the effect of NaClO solution on the corrosion resistance of stainless steel [12-16].

This work aims to investigate the effect of disinfection and/or cleaning of AISI 316L by hypochlorite solution on its corrosion behaviour as a function of NaClO concentration, pH and temperature. Electrochemical, photoelectrochemical and impedance measurements are carried out to study the change in the passive film composition as a function of immersion time in the cleaning/disinfection solution. The investigation is also supported by X-ray Photoelectron Spectroscopy.

2 - Experimental

Passive films were grown by immersion at open circuit potential on 316L/EN 1.4404 (0.02 wt.% C, 18 wt.% Cr, 10 wt.% Ni, 3 wt.% Mo, Fe balance) stainless steel. Samples were passivated in 60 mgL^{-1} (~ $8.1\ 10^{-4}$ M, pH ~ 8.5), 6 gL^{-1} (~ $8.1\ 10^{-2}$ M, pH ~ 10.8), and 60 gL^{-1} (~ 0.81 M, pH ~ 11.4) NaClO containing solutions for different immersion time (15 h, 24 h and 168 h) both at room

temperature and 45 °C. The aforementioned solutions were prepared by diluting a pure ~ 10% vol. NaClO solution. SS coupons were mechanically treated using grinding papers from P120 up to P1200 grit and were finally polished with a mixture of water, soap and ethanol coupled with 6μm and 1μm grinding papers in order to obtain a mirror surface finishing. SSs coupons were finally ultrasonically cleaned in ethanol and rinsed with deionized water. *In-situ* potential vs. time curves were recorded for 168 hours in the investigated solutions at both temperatures in order to study the early passivation stage and therefore to estimate the corrosion potential (E_{corr}) of 316L in the mimicking environments. Current vs. potential curves for passive films grown on 316L samples after different immersion time were recorded in 0.1 M Ammonium Biborate (ABE, pH ~ 8) aqueous solutions by sweeping the potential at 1 mV s^{-1} in the anodic direction from hydrogen evolution reaction. Photoelectrochemical characterization was carried out in 0.1 M ABE aqueous solutions using a 450 W UV−vis xenon lamp, coupled with a monochromator, allowing irradiation of the specimen through a quartz window. A two phase, lock-in amplifier, with a mechanical chopper, enables separation of the photocurrent, I_{ph}, from the total current in the cell. Photocurrent vs wavelength curves for $\lambda \geq 400$ nm were recorded using a 400 nm cut off filter.

XPS analysis was carried out using a Physical Electronics 5600 spectrometer (PHI 5600 XPS device) with a monochromated Al Kα radiation (1486.6 eV, 300 W) and a take-off angle of the emitted photoelectrons of 45° relative to the surface. Charging of the sample was corrected by using the C1s signal. Background subtraction and data evaluation were done by the MultiPak-Software (MultiPakV6.1A, 99 June 16, copyright Physical Electronics Inc., 1994–1999). The following core levels were analysed: Fe 2p, Cr 2p and O 1s. No peaks were detected in the Mo 3d and Ni 2p core level regions showing that Mo and Ni from the substrate are fully attenuated by the surface oxide film and that, if present in the oxide layer, their contents are below the detection limit of XPS (~0.5 at%). Electrochemical impedance spectroscopy (EIS) data were obtained using a Zahner Elektrik IM6ex controlled by a computer via Thales software. Impedance measurements were recorded at the open circuit potential in 0.1 M ABE (pH ~ 8) aqueous solutions by applying a sinusoidal signal of amplitude 10 mV over the frequency range 0.1 Hz – 100 kHz. Open circuit potential was recorded for 1 hour before recording EIS spectra. Experimental data were finally fitted by Thales software. A three-electrode arrangement was used, consisting of the specimen as working electrode, Pt as the counter and a silver/silver chloride (E_0 = 0.215 V/SHE) as reference electrode. Photoelectrochemical and impedance measurements were recorded in an exploited potential range narrow to the open circuit potential in order to not modify passive films composition due to anodic polarization.

3 - Results and discussion

To monitor the passive film properties as a function of the immersion time, AISI 316L coupons were immersed in NaClO solutions of different concentrations at room temperature and at 45°C. Figure 1 shows the open circuit potential vs immersion time plots recorded for 316L samples immersed in hypochlorite solution of different NaClO concentrations (and thus pH). At room temperature (see Figure 1a) an open circuit potential close to ~ 0.2 V vs. Ag/AgCl was measured in 60 mg L^{-1} solution (pH ~ 8.5) after 168 h of immersion. More anodic values were measured in 6 g L^{-1} (pH ~ 10.8) and 60 g L^{-1} (pH ~ 11.4) solutions reaching 0.45 and 0.62 V vs. Ag/AgCl, respectively, after 168 h of immersion. This can be explained by the very high oxidizing potential of highly concentrated NaClO solution. Indeed, in aerated ClO^- containing solution the possible cathodic processes can be:

$$Cl^- + H_2O = ClO^- + 2H^+ + 2e^- \quad (1a)$$

$$U_{eq} = 1.715 - 0.0591pH + 0.0295\log (ClO^-/Cl^-) \quad (V \text{ vs. SHE})$$

$$Cl_2 + 2H_2O = 2ClO- + 4H^+ + 2e^- \quad (1b)$$

$$U_{eq} = 2.036 - 0.1182pH + 0.0295\log ((ClO^-)^2/(Cl_2)) \quad (V \text{ vs. SHE})$$

$$4OH^- = O_2 + 2H_2O + 4e^- \quad (1c)$$

$$U_{eq} = 1.23 - 0.059pH \quad (V \text{ vs. SHE})$$

The corresponding equilibrium potentials, reported in table 1, show that hypochlorite reduction is thermodynamically favourable with respect to O_2 reduction. This shifts the corrosion potential toward more anodic values with respect to those measured at the same pH in ClO^- free solution. According to [17-18], corrosion potentials of 0 V vs. Ag/AgCl at pH ~ 8.4 and of - 0.5 V vs. Ag/AgCl at pH ~ 13 were measured for 316L samples. At the lowest ClO^- concentration (i.e. 60 mg L^{-1} and pH ~ 8.5), the resulting E_{corr} falls in the passive region according to Fig. S1, while at higher hypochlorite concentration the corrosion potentials are very close or higher than the equilibrium potential for Cr_2O_3 oxidation to chromate ions, since the early stage of immersion with consequent dissolution of Cr species from the passive film (see table 2). For the latter, E_{corr} increases monotonically with immersion time, so that also O_2 evolution becomes thermodynamically possible after 168 hours of immersion.

When the NaClO solution is at 45°C, a slightly lower corrosion potential is measured in 60 mg L^{-1} solution, while more anodic values (up to 0.8 V vs Ag/AgCl) were measured in 6 and 60 g L^{-1} solutions (see Figure 1b). The equilibrium potential for 1a, 1b and 1c at 45°C are not far from those at room temperature, since very low temperature coefficient can be estimated for the corresponding

reactions [19]. Thus, E_{corr} is significantly higher than the chromate formation potential and, for long immersion time, for oxygen evolution.

Fig. 2 and Fig 3 show Fe $2p_{3/2}$, Cr $2p_{3/2}$ and O 1s core level spectra after 168 h of immersion time in all passivating solutions at room temperature and at 45 °C. For the samples immersed at room temperature in 60 mg L^{-1} and 6 g L^{-1} of NaClO solution the Fe $2p_{3/2}$ core level spectra exhibit a peak at ~ 710 eV associated to Fe^{3+} in the surface oxide layer [20]. In the case of sample immersed in 60 g L^{-1} of NaClO solution, a shift of this peak toward higher binding energy (~ 712 eV) is evident and can be associated to the presence of Fe^{3+} hydroxide in the surface oxide layer [20]. It is important to mention that for the sample after 168 h of immersion in 60 mg L^{-1} of NaClO solution, a weak peak at ~ 707 eV related to metallic Fe is detected [20]. This experimental finding suggests the formation of a very thin passive film that does not allow to fully attenuating the photoelectrons emitted by the substrate. Cr $2p_{3/2}$ core level spectra exhibit a peak at ~ 576 eV related to the Cr^{3+} in the surface oxide layer [20]. No Cr^{+6} peaks are detected. For 60 g L^{-1} of NaClO solution a reduction of the peak intensity occurs, associated to a reduction of chromium content in the surface oxide layer. O 1s core level spectra exhibit one peak at ~ 530 eV that is related to O^{2-} and one peak at ~ 532 eV that is related to OH^{-}. For the samples immersed in 60 mg L^{-1} and 6 g L^{-1} of NaClO solution, the O^{2-} peak is higher with respect to OH^{-}. In the case of 60 g L^{-1} of NaClO solution, an increase of the OH^{-} with respect to O^{2-} peak is evident, relating to an increase of hydroxide content in the surface oxide layer in agreement with the Fe $2p_{3/2}$ core level spectra evidence.
The same peaks are present for the samples immersed in 60 mg L^{-1} and 6 g L^{-1} of NaClO solution at 45°C. In the case of 60 g L^{-1} of NaClO solution at 45°C, it is important to stress the absence of peak related to Cr^{3+} in the surface oxide layer and the increase of OH^{-} peak suggesting the hydration of the iron oxide on the surface.
Notably, we have calculated the intensity ratio between the principal peaks related to Fe and Cr in order to understand, if long exposure to chlorine environments could affect passive films composition and therefore electronic properties and corrosion resistance of passive layers (see table 3). According to the atomic composition of the passive layers grown on 316L surface after 168 h exposure, Cr/Fe ratio was calculated at both temperatures. A lower ratio was found by increasing the NaClO amount in disinfectant solutions. The same was found after long immersion time at 45 °C. This experimental finding suggests that the use of highly chlorine concentrated solutions cause iron enrichment in passive layers. due to chromium dissolution after long immersion time.

Soon after immersion in NaClO solution, polarization curves were recorded in a non-aggressive solution (0.1 M ABE), in order to get further information on the passive film formed during the

immersion in disinfection solutions. The passivity current is not strongly influenced by immersion time for 60 mg L^{-1} NaClO solution even at 45°C (see Fig. 4), and the effect is also negligible for 6 g L^{-1} solution at room temperature (see Fig. 5a). Conversely, at 45°C in 6 g L^{-1} and for 60 g L^{-1} solution at room temperature and 45°C, the passivity current is very low. Moreover, the peak current corresponding to Cr dissolution as Cr(VI) for passive film formed after 168 h in 60 g L^{-1} solution at 45°C becomes almost negligible suggesting a strong chromium depletion in the film (see Fig.6b).

In order to study the passive films composition and their electronic properties (band gap, conductivity type), photoelectrochemical measurements were carried out. Fig. 7a-b shows the photocurrent spectra recorded in 0.1 M ABE solution at U_E = 0.15 V vs. SSC (close to the open circuit potential in this solution) for passive films grown after 168 h of immersion in 60 mg L^{-1}, 6 g L^{-1} and 60 g L^{-1} at room temperature. According to Pourbaix Diagram at this potential and at this pH, the chromium oxide is thermodynamically stable. For passive film grown at pH 10.8 and 11.4, a photocurrent tail was also recorded for $\lambda \geq 400$ nm using a 400 nm cut off filter. Assuming non direct optical transitions, it is possible to estimate the band gap values shown in Figure 7c-d, as also reported in previous works [18, 21], according to the following equation:

$$(Q_{ph}\, h\nu)^{0.5} \propto (h\nu - E_g) \qquad (1)$$

where, for photon energy in the vicinity of band gap, Q_{ph}, the photocurrent yield, is proportional to the light absorption coefficient, $h\nu$ is the photon energy and E_g is the optical band gap.
The same photoelectrochemical investigation was carried out for passive films grown on 316L SS in the same passivation solutions at 45 °C. According to photocurrent spectra reported in Fig. 8a-b, passive films grown after 168 h of exposure at 45 °C in 6 g L^{-1} and 60 g L^{-1} are more photoactive than that grown at room temperature and a red shift of the light absorption threshold is evident.

Band gaps of passive films grown at the open circuit potential after different immersion times at different NaClO concentrations are listed in Tab. 4. E_g values are lower with respect to the band gap of Cr_2O_3 [18] as well as with respect to that estimated for the native oxide film (E_g close to 3.0 eV, [17, 21]. For passive films formed on AISI 316L in 60 mg L^{-1} at room temperature E_g ~ 2.85 eV almost independent on the immersion time, supporting the formation of an iron containing chromium oxide [18]. Slightly lower values were estimated for passive films grown at 45°C that can be explained by the formation of a more hydrated layer in agreement with the XPS results.

The band gap values estimated at higher NaClO concentrations at both room temperature and 45°C are significantly lower, suggesting the formation of iron rich hydrated passive films. Indeed, a band

gap value close to that reported for FeOOH [22] and band gap value ranging from 1.9 to 2.2 eV are reported for Fe_2O_3 [21, 23].

In order to check the sign of photocurrent and the conductivity type of the passive films, current vs time curves were recorded at U_E = 0.15 V vs SSC in 0.1 M ABE solution, by manually chopping sample irradiation under monochromatic light (λ = 280 nm). According to the current transient reported in Fig. 9 and Fig. 10, passive films grown on mechanically treated 316L SS samples after 168 h of immersion in the investigated solutions at both temperatures are n-type semiconductors, thus they are stable against anodic dissolution unless the presence of highly oxidizing species push them working under transpassive conditions. Anodic photocurrent spikes were measured at higher sodium hypochlorite concentrations, as expected for iron oxide layers [21].

EIS spectra were recorded in a slightly alkaline non-aggressive solution (0.1 M ABE) at the open circuit potential (U_{OC} ~ 0.1 V vs. SSC) in order to minimize the change in the films due to polarization. Fig. 11 shows the impedance spectra in the Nyquist representation as a function of NaClO concentration after 168 h of immersion at room temperature and at 45°C. EIS spectra of native oxide grown on 316L by air exposure is also reported for comparison. The dependence of the imaginary impedance component on real component is described by a portion of a slightly depressed semicircle, thus EIS spectra were fitted according to the equivalent circuit reported in Fig. 11 (see inset), where R_{el} is the electrolyte resistance, R_{ox} the resistance of the corresponding oxide film grown on 316L SS, *CPE* the constant phase element introduced in order to model the non ideal capacitance of the interface under investigation and *n* is the exponent of the *CPE* element [21]. According to the fitting parameters reported in Tab. 6, R_{ox} is higher than that obtained for the native oxide grown by air exposure (see Tab. 5) and their values increase by increasing both immersion time and NaClO concentration in simulating solutions. Application of the power-law model analysis [24-25] to CPE parameters given in Table 6 assuming ε = 12 and limiting value of resistivity of 450 Ohm cm taken from calibration of Fe17Cr stainless steel [25], allows to estimate the film thickness reported in the same Table 6. According to the power law approach passive films grown in 60 mg L^{-1} solution are thicker than those grown at higher NaClO concentration in contrast to the results provided by the XPS analyses. However, since the latter are n-type semiconductors with a very low Cr concentration, it is likely that the power law formula provides the space charge region width instead of the entire film thickness.

The experimental findings of this work suggest that disinfection in highly concentrated NaClO solution can lead to a strong chromium depletion of the passive film with consequent onset of Class II rouging phenomena. The passive film during immersion in 6 and 60 g L^{-1} NaClO solution loses

chromium with consequent formation of an iron rich hydrated oxide, which is a n-type semiconductor but under very high anodic potential (as those measured in this electrolyte) is under Fermi level pinning with consequent onset of a potential dependent current dissolution (see scheme of Fig. 12). Moreover, since the reduction of ClO^- ions produces chloride ions, a localized attack (i.e. pitting) can occur on the surface of the SS, whose pitting resistance is less than expected for the untreated material, due to the chromium depletion. This phenomenon can be enhanced by using a higher temperature (namely 45°C), due to a higher chromium dissolution rate as well as a to a reduction of pitting potential [26]. When the disinfection is carried out at pH 8.5, the film is a n-type semiconductor under reverse bias regime with a low passivation current balanced by the dissolution at the metal/film interface, thus accounting for a constant film thickness.

In ref. [10] the passive films on SS grown during immersion in NaClO solution are described by a topotactic model with chromium rich regions of insulating (or semiconducting) behaviour and iron rich regions based on magnetite with a high conductivity and, thus, where no charge accumulation is possible. The model accounts for a very high capacitance estimated from the impedance spectra corresponding to a film thickness without any physical meaning. However, the experimental findings of this work suggest a different model for the passive films grown in the disinfection solution. The EIS spectra can be easily fitted with just one time constant and the corresponding capacitance, estimated using the power law of ref. [24-25], provides physically reasonable thickness. Moreover, the corrosion potential reached during the immersion in 6 and 60 g L^{-1} NaClO solutions is so positive that the presence of magnetite is not likely.

4 - Conclusions

Passivation at open circuit potential was carried out by immersion in different NaClO containing solutions in order to simulate disinfection processes. The effect of chlorine concentration, exposure time and temperature on passivation kinetics was studied. According to the photoelectrochemical characterization of passive films grown on 316L SS, we have found that long time exposure to disinfectant solutions lead to the formation of iron – chromium mixed oxide films with an iron content that increases by increasing exposure time to aggressive environment, as suggested by XPS data. This experimental finding is also supported by PCS measurements. Estimated band gap decreases by increasing immersion time and NaClO concentration up to values corresponding to the formation of a hydrated iron oxide film. According to the photocurrent transients, passive films grown after immersion in simulating solutions are n-type semiconductor, and therefore more resistant toward anodic dissolution processes. In spite of their very low chromium content, the oxide resistance of passive films, estimated by fitting of EIS spectra, is very high even after long exposure

time to highly chlorine containing environment.

Acknowledgements

The authors thank Helga Hildebrand for conducting the XPS measurements.

5 – References

[1] Y. Chisti, Modern system of plant cleaning, in Encyclopedia of Food Microbiology, R. Robinson, C. Batt, P. Patel (Eds.), Academic Press, London, 1999, pp. 1806 – 1815.

[2] R.A. Corbett, Rouging-a discoloration of stainless steel surfaces, Mater. Perform. 40 (2001) 64-66.

[3] D.L. Roll, J.J. Kilkeary, Rouge detection & control, Chem. Eng. 108 (2001) 101-104.

[4] S. Fukuzaki, Mechanism of Actions of Sodium Hypochlorite in Cleaning and Disinfection Processes, Biocontrol Sci. 11 (2006) 147 – 157. https://doi.org/10.4265/bio.11.147.

[5] S. Fukuzaki, H. Urano, The Mode of Action of Sodium Hypochlorite in the Cleaning Process, Biocontrol Sci. 10 (2005) 21 – 29.

[6] X. Wang, J. Ma, Z. Wang, H. Chen, M. Liu, Z. Wu, Reinvestigation of membrane cleaning mechanisms using NaOCl: Role of reagent diffusion, J. Membr. Sci. 550 (2018) 278 – 285. https://doi.org/10.1016/j.memsci.2017.12.083.

[7] I. B. Gomesa, M. Simões, L.C. Simões, The effects of sodium hypochlorite against selected drinking water-isolated bacteria in planktonic and sessile states, Sci. Total Environ. 565 (2016) 40 – 48. https://doi.org/10.1016/j.scitotenv.2016.04.136.

[8] Y. Qi, J. Li, R. Liang, S. Ji, J. Li, M. Liu, 2017. Chemical additives affect sulfate reducing bacteria biofilm properties adsorbed on stainless steel 316L surface in circulating cooling water system, Front. Env. Sci. Eng. 11, 14. https://doi.org/10.1007/s11783-017-0917-7.

[9] G. Sirtes, T. Waltimo, M. Schaetzle, M. Zehnder, The effects of temperature on sodium hypochlorite short-term stability, pulp dissolution capacity, and antimicrobial efficacy, J. Endod. 31 (2005) 669 – 671. https://doi.org/10.1097/01.don.0000153846.62144.d2

[10] B. Guitan, X.R. Novoa, B. Puga, Electrochemical Impedance Spectroscopy as a tool for materials selection: Water for haemodialysis, Electrochim. Acta 56 (2011) 7772 – 7779. https://doi.org/10.1016/j.electacta.2011.03.055

[11] R.H. Schmidt, Basic Elements of Equipment Cleaning and Sanitizing in Food Processing and Handling Operations, IFAS Extension, July 2014.

[12] D. Vázquez-Sánchez, M.L. Cabo, P.S. Ibusquiza, J.J. Rodríguez-Herrera, Biofilm-forming ability and resistance to industrial disinfectants of Staphylococcus aureus isolated from fishery products, Food Control 39 (2014) 8 – 16. https://doi.org/10.1016/j.foodcont.2013.09.029.

[13] D. Vázquez-Sánchez, J.A. Galvão, M. Oetterer, Contamination sources, serogroups, biofilm-forming ability and biocide resistance of Listeria monocytogenes persistent in tilapia-processing facilities, J. Food Sci. Technol., 54 (2017) 3867 – 3879. https://doi.org/10.1007/s13197-017-2843-x.

[14] X. Chen, Y.C. Hung, Effects of organic load, sanitizer pH and initial chlorine concentration of chlorine-based sanitizers on chlorine demand of fresh produce wash waters, Food Control 77 (2017) 96 – 101. https://doi.org/10.1016/j.foodcont.2017.01.026.

[15] M. Santos Rosado Castro, M. da Silva Fernandes, D.Y. Kabuki, A.Y. Kuaye, 2018. Biofilm formation of Enterococcus faecium on stainless steel surfaces: Modeling and control by disinfection agents. J. Food Process Eng. 41, e12663. https://doi.org/10.1111/jfpe.12663.

[16] J.G.P. Martin, G. de Oliveira e Silva, C.R. da Fonseca, C.B. Morales, C. Souza Pamplona Silva, D.L. Miquelluti, E. Porto, Efficiency of a cleaning protocol for the removal of enterotoxigenic Staphylococcus aureus strains in dairy plants, Int. J. Food Microbiol. 238 (2016) 295 – 301. https://doi.org/10.1016/j.ijfoodmicro.2016.09.018.

[17] M. Santamaria, F. Di Franco, F. Di Quarto, M. Pisarek, S. Zanna, P. Marcus, Photoelectrochemical and XPS characterisation of oxide layers on 316L stainless steel grown in high-temperature water, J. Solid State Electrochem. 19 (2015) 3511 – 3519. https://doi.org/10.1007/s10008-015-2849-0.

[18] G. Tranchida, M. Clesi, F. Di Franco, F. Di Quarto, M. Santamaria, Electronic properties and corrosion resistance of passive films on austenitic and duplex stainless steels, Electrochim. Acta 273 (2018) 412 - 423. https://doi.org/10.1016/j.electacta.2018.04.058.

[19] A.J. deBethune, T.S. Licht, N. Swendeman, The Temperature Coefficients of Electrode Potentials. The Isothermal and Thermal Coefficients – The Standard Ionic Entropy of Electrochemical, Transport of the Hydrogen Ion, J. Electrochem. Soc. 106 (1959) 616 – 625. https://doi.org/10.1149/1.2427449.

[20] Z. Wang, F. Di Franco, A. Seyeux, S: Zanna, V. Maurice, P. Marcus, Passivation – Induced Physicochemical Alterations of the Native Surface Oxide Film on 316L Austenitic Stainless Steel, J. Electrochem. Soc. 166 (2019), C3376 - C3388. https://doi.org/10.1149/2.0321911jes.

[21] F. Di Franco, M. Santamaria, G. Massaro, F. Di Quarto, Photoelectrochemical monitoring of rouging and de – rouging on AISI 316L, Corros. Sci. 116 (2017) 74 – 87. https://doi.org/10.1016/j.corsci.2016.12.016

[22] L. Song, X. Ma, Z. Chen, B. Hou, The role of UV illumination on the initial atmospheric corrosion of 09CuPCrNi weathering steel in the presence of NaCl particles, Corros. Sci. 87 (2014) 427 – 437. https://doi.org/10.1016/j.corsci.2014.07.013.

[23] M. Santamaria, S. Terracina, Y. Konno, H. Habazaki, F. Di Quarto, Physicochemical characterization and photoelectrochemical analysis of iron oxide films, J. Solid State Electrochem. 17 (2013) 3005 – 3014. https://doi.org/10.1007/s10008-013-2131-2.

[24] B. Hirschorn, M.E. Orazem, B. Tribollet, V. Vivier, I. Frateur, M. Musiani, Constant-phase-element behavior caused by resistivity distributions in films: I. Theory, J. Electrochem. Soc. 157 (2010) C452 – C457. https://doi.org/10.1149/1.3499565.

[25] M.E. Orazem, I. Frateur, B. Tribollet, V. Vivier, S. Marcelin, N. Pébère, A.L. Bunge, E.A. White, D.P. Riemer, M. Musiani, Dielectric properties of materials showing constant-phase-element (CPE) impedance response, J. Electrochem. Soc. 160 (2013) C215–C225. https://doi.org/10.1149/2.033306jes.

[26] L.L. Shreir, Corrosion, second ed., Newnes 1976.

Figure Captions

Fig. 1. Potential vs time curves recorded for 168 hours of immersion in 60 mgL^{-1} (pH ~ 8.4) (red line), 6 gL^{-1} (pH ~ 10.8) (green line) and 60 gL^{-1} (pH ~ 11.4) (blue line) at a) room temperature and b) 45°C.

Fig. 2. Fe $2p_{3/2}$, Cr $2p_{3/2}$ and O 1s core level spectra after 168 h exposure at room temperature in 60 mgL^{-1} (blue line), 6 gL^{-1} (red line) and 60 gL^{-1} (green line) NaClO containing solutions.

Fig. 3. Fe $2p_{3/2}$, Cr $2p_{3/2}$ and O 1s core level spectra after 168 h exposure at 45 °C in 60 mgL^{-1} (blue line), 6 gL^{-1} (red line) and 60 gL^{-1} (green line) NaClO containing solutions.

Fig. 4. Polarization curves recorded at 1 mV s^{-1} in 0.1 M ABE (pH ~ 8) after passivation at the open circuit potential in 60 mg L^{-1} NaClO at a) room temperature and b) 45°C.

Fig. 5. Polarization curves recorded at 1 mV s^{-1} in 0.1 M ABE (pH ~ 8) after passivation at the open circuit potential in 6 g L^{-1} NaClO at a) room temperature and b) 45°C.

Fig. 6. Polarization curves recorded at 1 mV s^{-1} in 0.1 M ABE (pH ~ 8) after passivation at the open circuit potential in 60 g L^{-1} NaClO at a) room temperature and b) 45°C.

Fig. 7. Raw photocurrent spectra related to passive films grown on 316L SS with a mirror surface finishing after 168 h of immersion at room temperature in disinfection solutions by polarizing samples in 0.1 M ABE solution (pH ~ 8) at $U_E = 0.15$ V vs. Ag/AgCl for (a) $0 < \lambda < 200$ nm and (b) $\lambda \geq 400$nm. (c) $(Q_{ph}\ hv)^{0.5}$ *vs* hv for passive film grown after 168 h of immersion in 60 mgL^{-1} NaClO, (d) $(Q_{ph}\ hv)^{0.5}$ *vs* hv for passive film grown after 168h of immersion in 6 gL^{-1} NaClO and (e) $(Q_{ph}\ hv)^{0.5}$ *vs* hv for passive film grown after 168h of immersion in 60 gL^{-1} NaClO.

Fig. 8. Raw photocurrent spectra related to passive films grown on 316L SS with a mirror surface finishing after 168 h of immersion at 45°C in disinfection solutions by polarizing samples in 0.1 M ABE solution (pH ~ 8) at $U_E = 0.15$ V vs. Ag/AgCl for (a) $0 < \lambda < 200$ nm and (b) $\lambda \geq 400$nm. (c) $(Q_{ph}\ hv)^{0.5}$ *vs* hv for passive film grown after 168 h of immersion in 60 mgL^{-1} NaClO, (d) $(Q_{ph}\ hv)^{0.5}$ *vs* hv for passive film grown after 168h of immersion in 6 gL^{-1} NaClO and (e) $(Q_{ph}\ hv)^{0.5}$ *vs* hv for passive film grown after 168h of immersion in 60 gL^{-1} NaClO.

Fig. 9. Current vs time curves recorded at $U_E = 0.15$ V vs SSC in 0.1 M ABE solution (pH ~ 8) at $\lambda = 280$ for passive grown on 316L SS mechanically treated after 168 h of immersion at room temperature in a) 60 mgL^{-1}, b) 6 gL^{-1} and c) 60 gL^{-1} NaClO in disinfectant solutions.

Fig. 10. Current vs time curves recorded at U_E = 0.15 V vs SSC in 0.1 M ABE solution (pH ~ 8) at λ = 280 nm for passive grown on 316L SS mechanically treated after 168 h of immersion at 45 °C in a) 60 mgL^{-1}, b) 6 gL^{-1} and c) 60 gL^{-1} NaClO in disinfectant solutions.

Fig. 11. EIS spectra in Nyquist representation for passive films grown on 316L SS after passivation at open circuit potential at a) room temperature and b) 45 °C, recorded in 0.1 M ABE solution (pH ~ 8) at the open circuit potential (U_{OC} ~ 0.1 V vs SSC).

Fig. 12. Scheme relating to passive film/electrolyte interface a) under anodic potential and b) under Fermi level pinning where allowed electronic states are reported in red.

Tables

	E_0 / V vs SSC		
	pH 8.4	**pH 10.8**	**pH 11.4**
(1a) ClO^- / Cl^-	1.104	1.023	1.017
(1b) ClO^- / Cl_2	0.838	0.672	0.660
(1c) O_2 / OH^-	0.534	0.393	0.357

Table 1. Equilibrium potentials for the three possible cathodic processes in the NaClO solutions at the corresponding pH.

	E_0 / V vs SSC		
Cr_2O_3/CrO_4^{--}	**pH 8.4**	**pH 10.8**	**pH 11.4**
$E_o = 1.386 - 0.0985pH + 0.0197\log(CrO_4^{2-})$	0.24	0	-0.06
$E_o = 1.311 - 0.0985pH + 0.0197\log(CrO_4^{2-})$	0.17	-0.07	-0.13
$E_o = 1.244 - 0.0985pH + 0.0197\log(CrO_4^{2-})$	0.10	-0.14	-0.197

Table 2. Equilibrium potentials for chromium oxidation to chromate ions at the corresponding pH.

Atomic percent (at.%)							
Room Temperature							
	N 1s	**O 1s**	**Cr 2p**	**Fe 2p**	**Ni 2p**	**Mo 3d**	**Cr / Fe**
60 mgL^{-1}	0.77	32.05	1.57	6.32	2.07	0.27	0.25
6 gL^{-1}	1.24	54.6	1.2	11.23	0	0.17	0.11
60 gL^{-1}	0.21	49.85	0.78	8.1	0.58	0.06	0.10
45 °C							
	N 1s	**O 1s**	**Cr 2p**	**Fe 2p**	**Ni 2p**	**Mo 3d**	**Cr / Fe**
60 mgL^{-1}	0.1	31.73	4.38	19.19	3.66	0.2	0.24
6 gL^{-1}	0.58	47.73	0.97	8.7	0.15	0.07	0.11
60 gL^{-1}	0.34	54.85	0.53	4.64	0	0.09	0.11

Table 3. Atomic composition of passive layers grown after 168 h of exposure in chlorine containing disinfection solutions at room temperature and at 45 °C. Cr / Fe atomic ratio is also reported as a function of passivation conditions.

E_g / eV						
Passivation conditions	**Room Temperature**			**45 °C**		
	15 h	**24 h**	**168 h**	**15 h**	**24 h**	**168 h**
60 mg L^{-1}	2.86	2.86	2.84	2.61	2.6	2.54
6 g L^{-1}	2.54	2.53	2.37	2.38	2.36	2.35
60 g L^{-1}	2.39	2.32	2.29	2.47	2.35	2.4

Table 4. Band gap values for passive films grown on 316L SSs with a mirror surface finishing at the open circuit potential by immersion for 15 h, 24 h and 168 h in different NaClO containing solutions both at room temperature and 45 °C.

native oxide				
R_{sol} Ω cm²	R_{ox} Ω cm²	Q S s^{α} cm^{-2}	α	δ nm
48.87	1.94E+05	1.46E-05	0.931	3.18

Table 5. Fitting parameters of EIS spectra on passive films grown by air exposure on 316L SS according to the equivalent circuit reported in the inset of Fig. 11.

Passivation conditions		Room Temperature					45 °C				
		R_{sol} Ω cm²	R_{ox} Ω cm²	Q S s^{α} cm^{-2}	α	δ nm	R_{sol} Ω cm²	R_{ox} Ω cm²	Q S s^{α} cm^{-2}	α	δ nm
60 mg L^{-1}	15 h	60.76	5.14E+05	1.14E-05	0.940	3.49	61.43	8.19E+05	6.28E-06	0.920	9.32
	24 h	49.63	1.96E+06	6.39E-06	0.904	6	59.46	1.65E+06	1.07E-05	0.942	3.59
	168 h	46.61	2.50E+06	8.54E-06	0.936	4.51	57.11	2.52E+06	1.56E-05	0.940	2.40
6 g L^{-1}	15 h	52.97	8.55E+05	1.61E-05	0.940	2.40	54.93	1.41E+06	1.13E-05	0.940	3.49
	24 h	58.27	2.13E+06	7.69E-06	0.932	6.17	54.26	2.01E+06	1.49E-05	0.942	2.56
	168 h	56.23	3.00E+06	1.30E-05	0.940	2.95	54.49	3.96E+06	1.45E-05	0.931	3.17
60 g L^{-1}	15 h	55.81	9.11E+06	1.89E-05	0.946	1.63	60.79	1.22E+07	1.76E-05	0.929	2.64
	24 h	64.09	9.50E+06	1.78E-05	0.940	2.13	55.26	1.60E+07	1.97E-05	0.937	2.08
	168 h	58.36	1.76E+07	1.75E-05	0.935	2.79	53.78	2.60E+07	1.62E-05	0.902	5.61

Table 5. Fitting parameters of EIS spectra on passive films grown on 316L SS at the open circuit potential by immersion in disinfectant solutions under investigation both at room temperature and 45 °C according to the equivalent circuit reported in the inset of Fig. 11. Thickness values estimated according to the power law are also reported.

Figure 1.

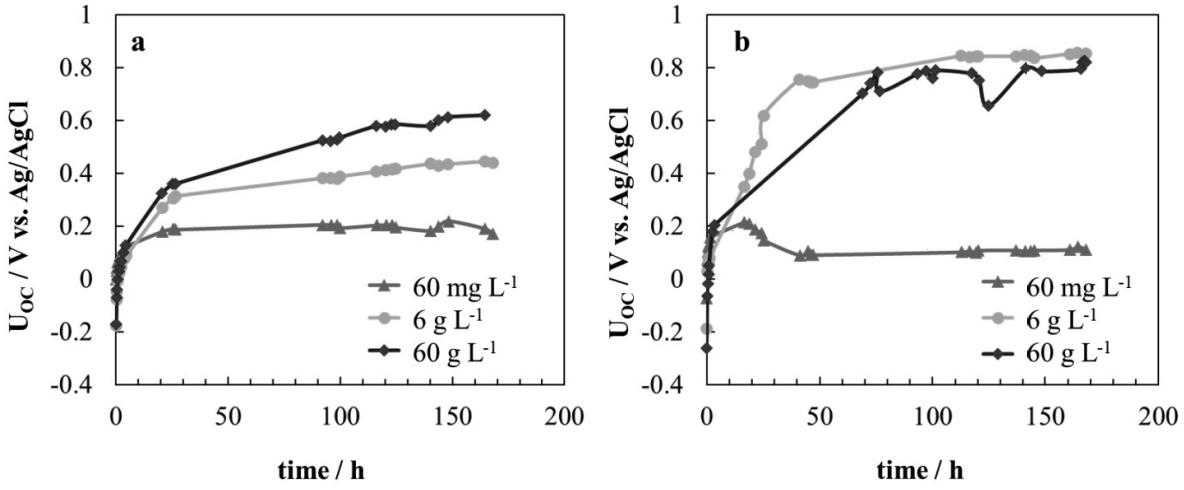
a
b
U_{OC} / V vs. Ag/AgCl
time / h
60 mg L-1
6 g L-1
60 g L-1
1
0.8
0.6
0.4
0.2
0
-0.2
-0.4
0
50
100
150
200

Figure 2.

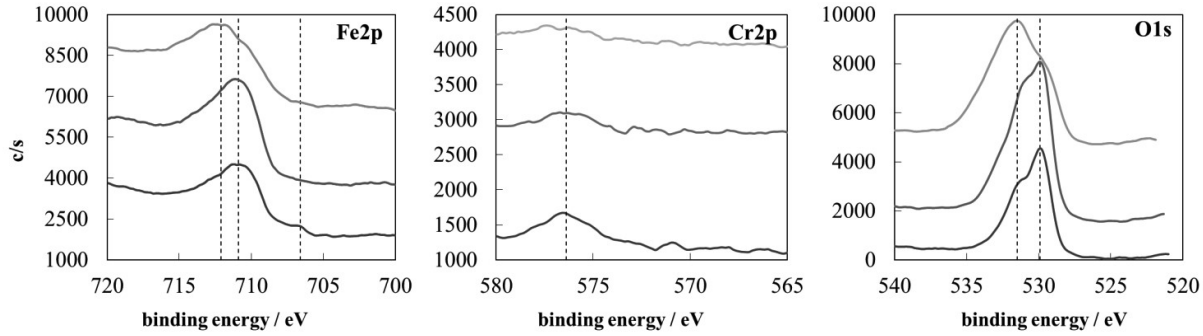
Fe2p
Cr2p
O1s
c/s
binding energy / eV
binding energy / eV
binding energy / eV

Figure 3.

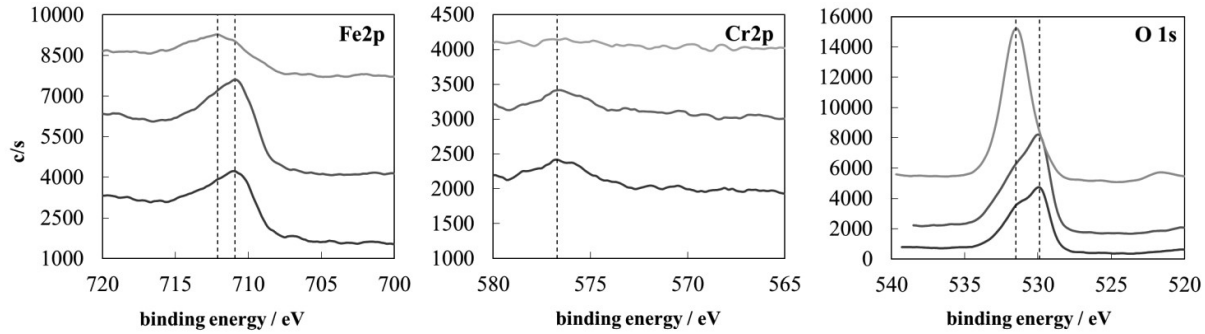
Fe2p
Cr2p
O 1s
c/s
binding energy / eV
binding energy / eV
binding energy / eV

Figure 4.

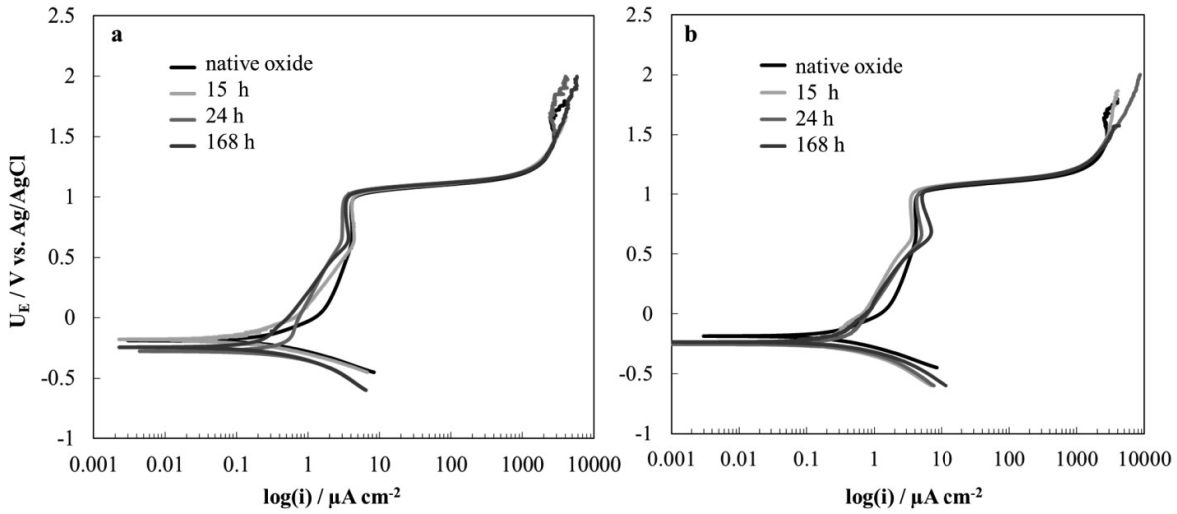
a
native oxide
15 h
24 h
168 h
U_E / V vs. Ag/AgCl
log(i) / µA cm^{-2}
b
native oxide
15 h
24 h
168 h
log(i) / µA cm^{-2}

Figure 5.

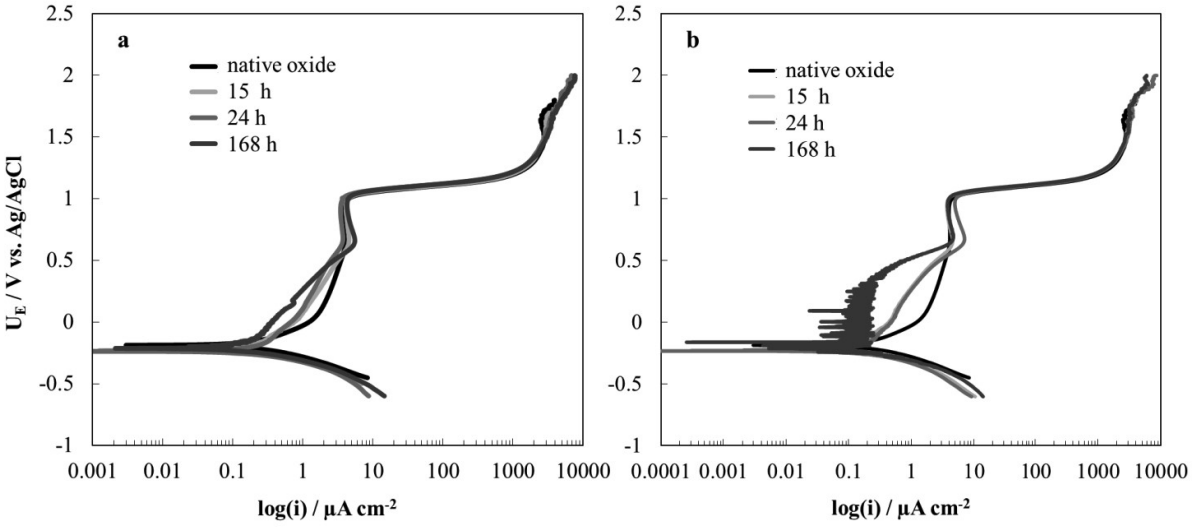
a
native oxide
15 h
24 h
168 h
U_E / V vs. Ag/AgCl
log(i) / µA cm^{-2}
b
native oxide
15 h
24 h
168 h
log(i) / µA cm^{-2}

Figure 6.

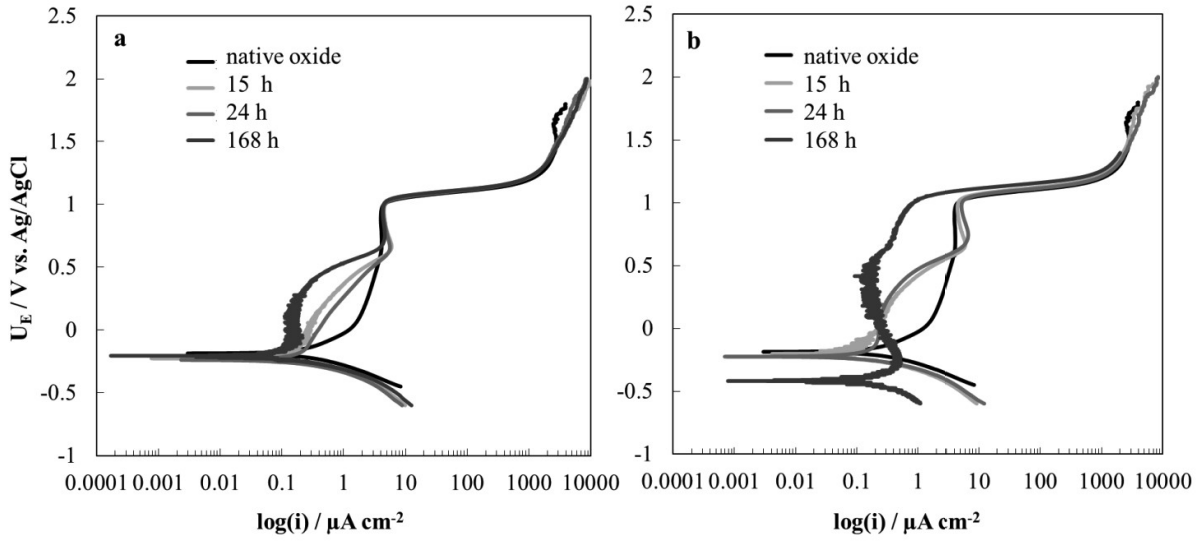
a
native oxide
15 h
24 h
168 h
U_E / V vs. Ag/AgCl
log(i) / µA cm^{-2}
b
native oxide
15 h
24 h
168 h
log(i) / µA cm^{-2}

Figure 7.

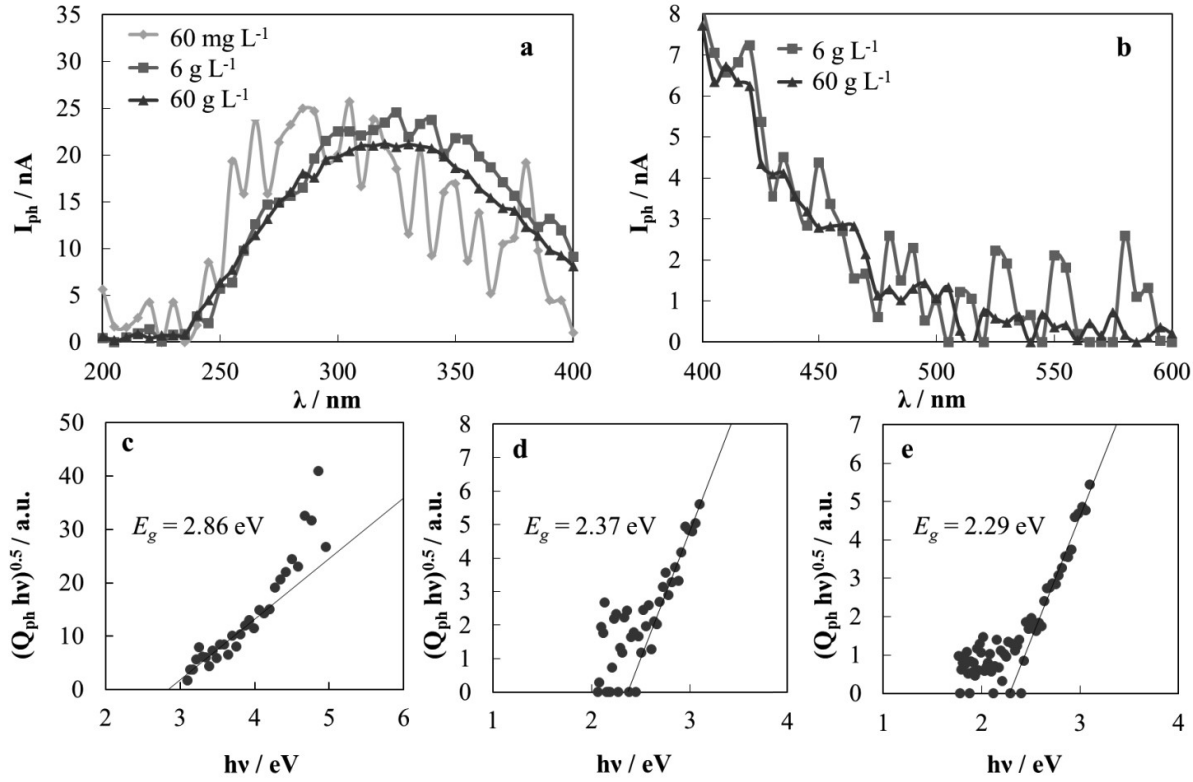
a
60 mg L-1
6 g L-1
60 g L-1
Iph / nA
λ / nm
b
6 g L-1
60 g L-1
Iph / nA
λ / nm
c
Eg = 2.86 eV
(Qph hν)0.5 / a.u.
hν / eV
d
Eg = 2.37 eV
(Qph hν)0.5 / a.u.
hν / eV
e
Eg = 2.29 eV
(Qph hν)0.5 / a.u.
hν / eV

Figure 8.

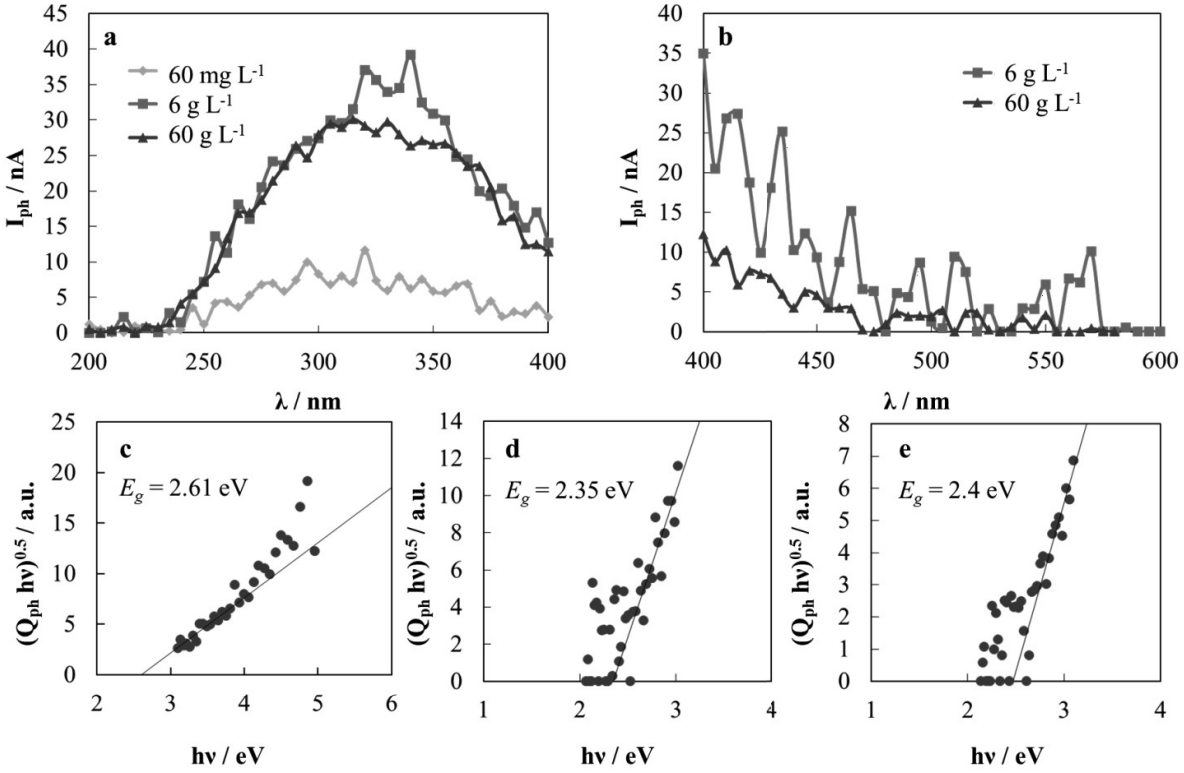
a
60 mg L-1
6 g L-1
60 g L-1
Iph / nA
λ / nm
b
6 g L-1
60 g L-1
Iph / nA
λ / nm
c
Eg = 2.61 eV
(Qph hν)0.5 / a.u.
hν / eV
d
Eg = 2.35 eV
(Qph hν)0.5 / a.u.
hν / eV
e
Eg = 2.4 eV
(Qph hν)0.5 / a.u.
hν / eV

Figure 9.

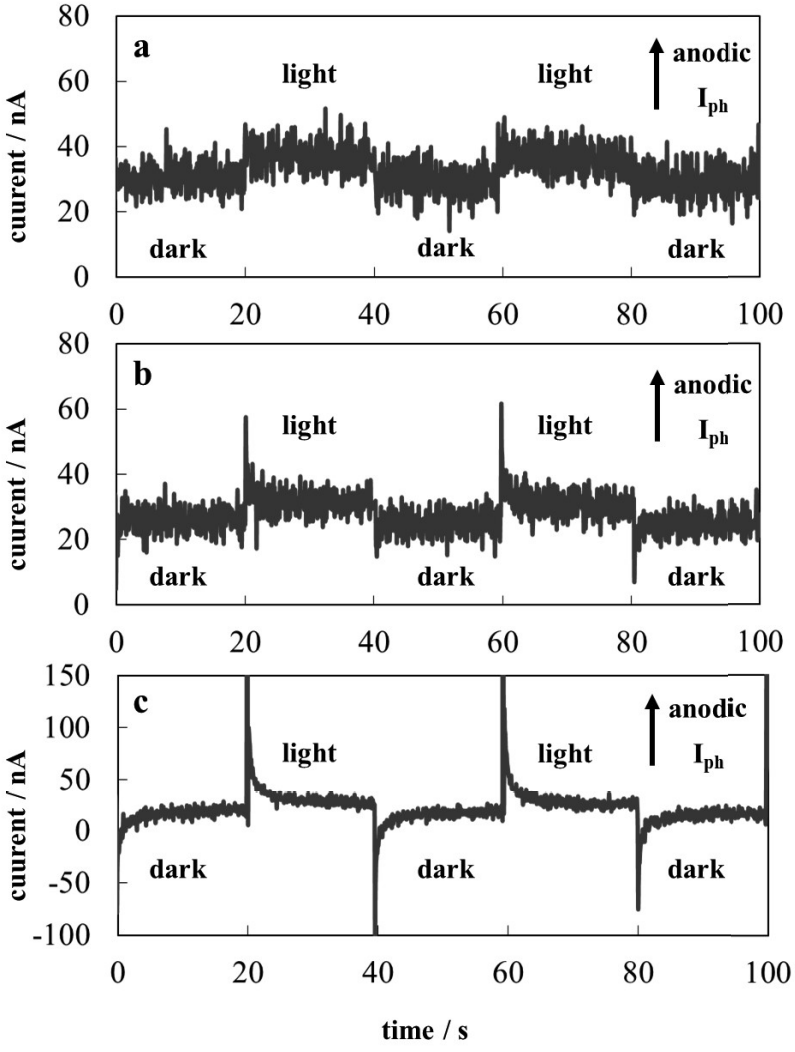
a
b
c
light
dark
anodic
I_{ph}
cuurent / nA
time / s
0
20
40
60
80
100
-100
-50
50
150

Figure 10.

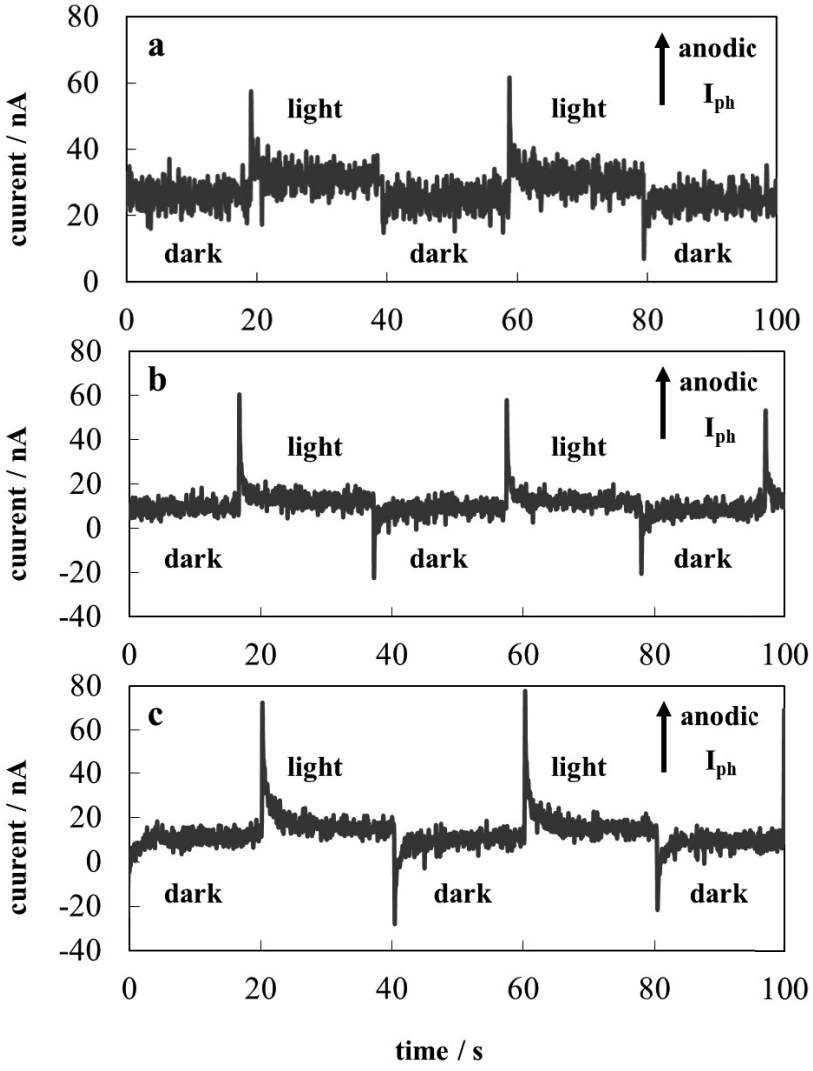
a
b
c
anodic
I_{ph}
light
dark
cuurent / nA
time / s
80
60
40
20
0
-20
-40
0
20
40
60
80
100

Figure 11.

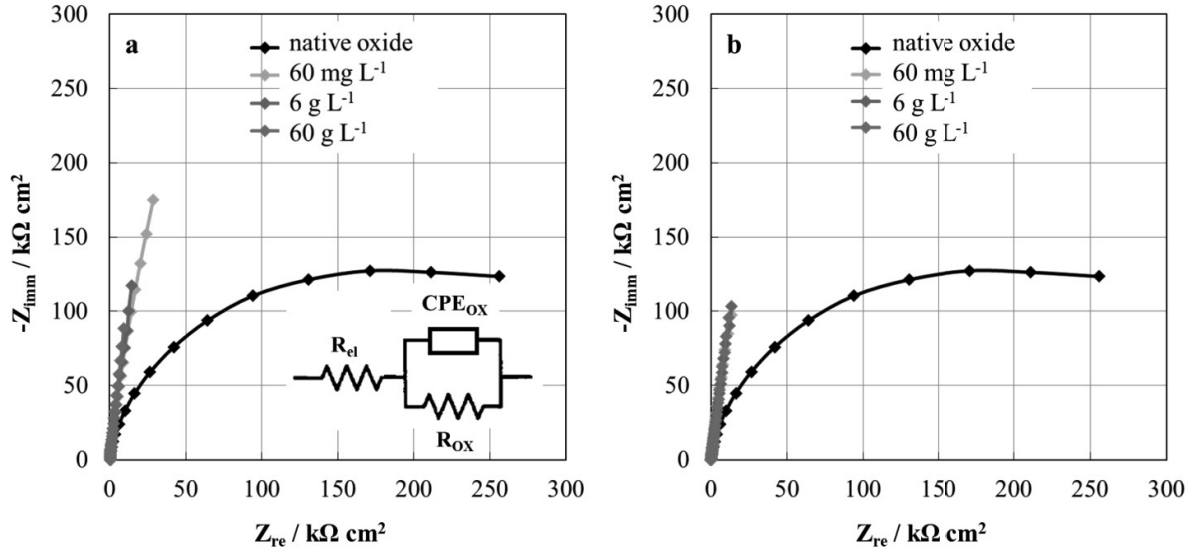
a
native oxide
60 mg L-1
6 g L-1
60 g L-1
CPEOX
Rel
ROX
-Zimm / kΩ cm2
Zre / kΩ cm2
b
native oxide
60 mg L-1
6 g L-1
60 g L-1
-Zimm / kΩ cm2
Zre / kΩ cm2

Figure 12.

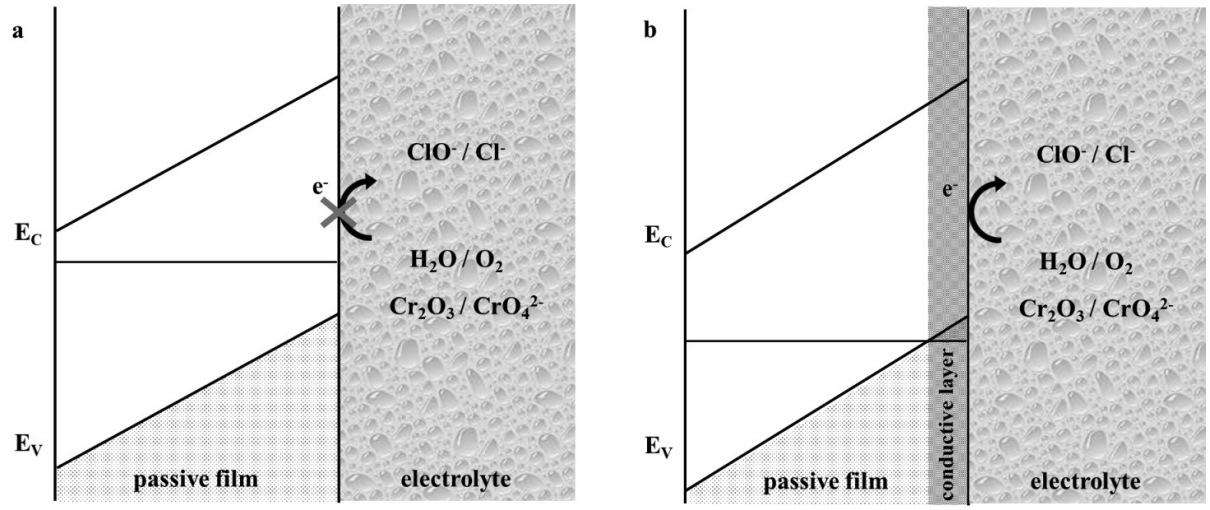
a
E_C
E_V
ClO^- / Cl^-
e^-
H_2O / O_2
Cr_2O_3 / CrO_4^{2-}
passive film
electrolyte
b
E_C
E_V
ClO^- / Cl^-
e^-
H_2O / O_2
Cr_2O_3 / CrO_4^{2-}
conductive layer
passive film
electrolyte

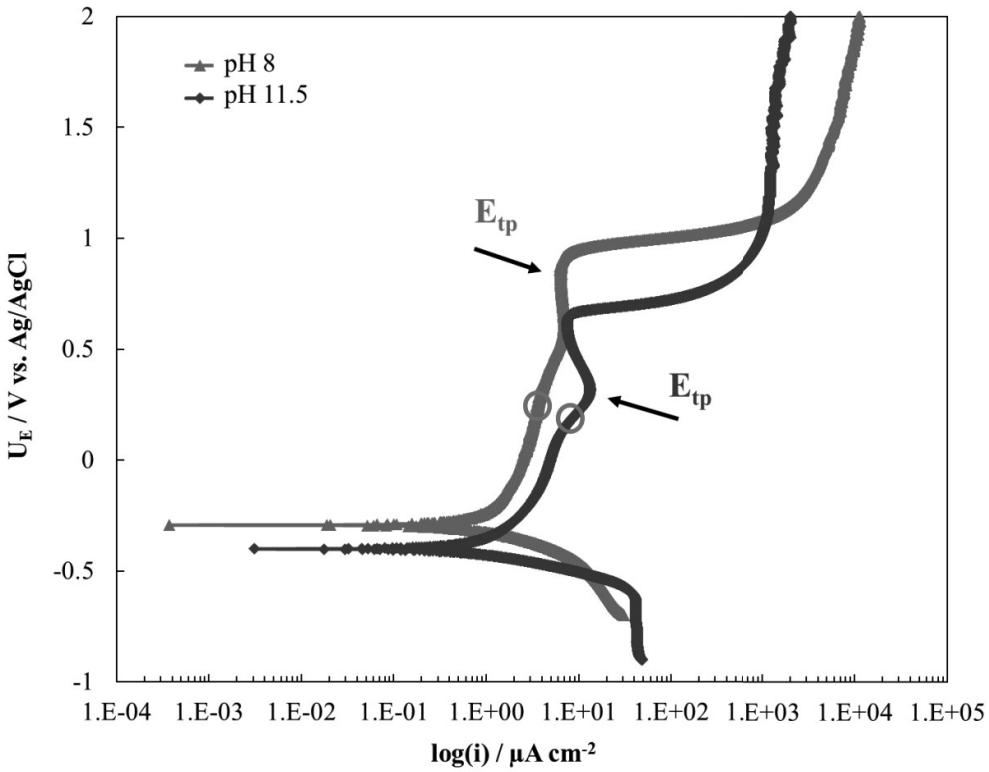

Fig. S1. Polarization curves recorded in a) 0.1 M ABE at pH 8 (red line) and b) 0.01 M NaOH pH 11.5 (blue line).